Showcasing research from Professor Scheschkewitz's laboratory at Saarland University (Germany).

Exohedral functionalization *vs.* core expansion of siliconoids with Group 9 metals: catalytic activity in alkene isomerization

Unprecedented rhodium and iridium incorporated siliconoids are readily accessible from the silylene-substituted Si_6 siliconoid and Group 9 metal fragments. The pending N-heterocyclic silylene ligand acts as a handle enabling unique coordination environments with up to five silicon atoms. In particular, the iridium species shows competitive catalytic activity in the isomerization of terminal alkenes to 2-alkenes.

As featured in:

ROYAL SOCIETY
OF **CHEMISTRY**

rsc.li/chemical-science

EDGE ARTICLE

Exohedral functionalization *vs.* core expansion of siliconoids with Group 9 metals: catalytic activity in alkene isomerization†

Nadine E. Poitiers, [ID] Luisa Giarrana, Volker Huch, Michael Zimmer and David Scheschkewitz [ID] *

Taking advantage of pendant tetrylene side-arms, stable unsaturated Si_6 silicon clusters (siliconoids) with the benzpolarene motif (the energetic counterpart of benzene in silicon chemistry) are successfully employed as ligands towards Group 9 metals. The pronounced σ-donating properties of the tetrylene moieties allow for sequential oxidative addition and reductive elimination events without complete dissociation of the ligand at any stage. In this manner, either covalently linked or core-expanded metallasiliconoids are obtained. $[Rh(CO)_2Cl]_2$ inserts into an endohedral Si–Si bond of the silylene-functionalized hexasilabenzpolarene leading to an unprecedented coordination sphere of the Rh centre with five silicon atoms in the initial product, which is subsequently converted to a simpler derivative under reconstruction of the Si_6 benzpolarene motif. In the case of $[Ir(cod)Cl]_2$ (cod = 1,5-cyclooctadiene) a similar Si–Si insertion leads to the contraction of the Si_6 cluster core with concomitant transfer of a chlorine atom to a silicon vertex generating an exohedral chlorosilyl group. Metallasiliconoids are employed in the isomerization of terminal alkenes to 2-alkenes as a catalytic benchmark reaction, which proceeds with competitive selectivities and reaction rates in the case of iridium complexes.

Introduction

The control of the reactivity of transition metal centres is a pivotal aspect of homogenous catalysis and therefore the development of novel ligands for transition metals is one of the priorities of organometallic chemistry. Unsaturated silicon compounds with the two major sub-categories of silylenes[1] and disilenes[1a,2] are typically characterized by a surplus of electrons and are therefore inherently stronger σ-donors than the corresponding carbon species, while retaining π-acceptor properties in some cases due to their unsaturated nature.[3] First applications in homogeneous catalysis include C–H borylation,[4] reduction of organic amides,[5] Sonogashira and Heck cross-coupling reactions[6] and hydrosilylation of ketones.[7]

Recently, a third widely occurring sub-category was introduced into the class of stable unsaturated silicon species, the so-called siliconoids, partially unsubstituted neutral silicon clusters.[8] Despite their unsaturated nature, applications of siliconoids as ligands towards transition metals are virtually unexplored. With our report on anionically functionalized Si_6

derivatives,[9] however, a conceptual link towards (poly)anionic, completely unsubstituted deltahedral Zintl anions of silicon[10] was established, which in fact exhibit a rich chemistry towards transition metals: silicides and their heavier congeners of germanium and tin have frequently been employed as extraordinarily electron-rich ligands towards transition metal centres,[11] and Zintl anions of Group 14 elements heavier than silicon can be converted to transition metal-centred derivatives $M@E_n^{x-}$.[12] In all reported cases, the negative charges of the polyanionic precursors are (at least partially) retained in the transition metal-containing products with often adverse consequences for their solubility and stability, limiting their application, *e.g.* in homogeneous catalysis. Siliconoids with their stabilizing shell of organic ligands and high solubility due to their charge-neutrality appear to be the logical choice to overcome both limitations.

The first transition metal-substituted siliconoids, *ligato*-hexasilabenzpolarenes Si_6–$Zr(Cp)_2Cl$ and Si_6–$Hf(Cp)_2Cl$ with the covalently attached metallocene moiety were disclosed just recently.[13] In contrast, the application of siliconoids as direct charge-neutral ligands towards transition metals has remained unsuccessful so far although the introduction of a silylene side-arm allowed for the coordination to $Fe(CO)_4$ moieties in the periphery of the hexasilabenzpolarene motif.[13] Now we show that by using the Group 9 metals rhodium and iridium a much larger variety of unprecedented coordination modes to

siliconoids can be realized. We demonstrate that covalent bonding modes between the metal and the uncompromised hexasilabenzpolarene scaffold are related to the endohedral incorporation of the metal centre into the siliconoid cluster in a reversible manner. Finally, with the isomerization of alkenes we provide a first proof-of-principle for the application of the thus prepared soluble transition metal/silicon hybrid clusters as homogenous catalysts.

Results and discussion
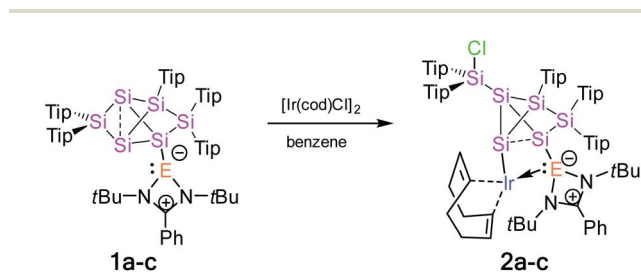
Synthesis of iridium complexes

Treatment of tetrylene-functionalized siliconoids **1a–c** with 0.5 equivalents of bis[(1,5-cyclooctadiene)iridium(I) chloride] affords the tetrylene-Si$_6$ iridium complexes **2a–c** in an NMR spectroscopically quantitative manner (Scheme 1). Complexes **2a–c** were fully characterized by X-ray diffraction on single crystals, elemental analysis, and multinuclear NMR spectroscopy.

The ^{29}Si NMR spectrum of **2a–c** shows six sharp resonances in a much narrower range than usual for hexasilabenzpolarenes (+175.4 to −279.0 ppm),[9] which provides a first hint at the rearrangement of the cluster scaffold and the ensuing loss of the spherical aromaticity and the associated magnetically induced cluster current. On the basis of the 2D ^{29}Si/^{1}H correlation NMR spectrum, the signals at 56.7 ppm (**2a**), 52.6 ppm (**2b**) and 50.2 ppm (**2c**) are assigned to the endohedral SiTip$_2$ moieties. The signals at 13.3 (**2a**), 12.8 (**2b**) and 12.2 ppm (**2c**) are very close in chemical shift to that of the exocyclic silicon atom in chlorosilyltricyclo[2.1.0.0^{2,5}]pentasilane (5.8 ppm)[14] and were therefore tentatively attributed to the extrusion of one SiTip$_2$ unit from the cluster core of **2a–c**. The resonances at −38.4 (**2a**), −41.5 (**2b**) and −42.1 ppm (**2c**) are assigned to the SiTip vertices. Most remaining ^{29}Si signals are observed at

a higher field (see ESI†) with the exception of one distinct resonance of **2a** at 33.4 ppm, which is apparently due to the pendant silylene centre (Table 1).

Single crystals of **2a–c** were obtained by crystallization from hexane in 68% (**2a**), 61% (**2b**) and 63% (**2c**) yield and the tricyclic structures of the siliconoid–iridium complexes were confirmed by X-ray diffraction in the solid state (Fig. 1). As anticipated on the basis of NMR data, the *privo*-vertex has been extruded from the cluster core due to the additional bond to the chlorine atom transferred from the iridium centre, which in turn is not only coordinated by the pendant tetrylene moiety but also by the former *nudo*-vertex of the benzpolarene starting material. The structural model of **2c** could not be refined in a satisfactory manner; the following discussion thus focuses on **2a,b**. The Ir–E bond lengths (E = Si, Ge, Sn; **2a**: Si3–Ir: 2.320(1) Å and Si7–Ir: 2.334(1) Å; **2b**: Si3–Ir: 2.3517(7) Å and Ge–Ir: 2.4113(3) Å) are those of single bonds.[16] The slightly longer distance between the pendant tetrylene and the iridium centre may be explained by the dative *vs.* covalent bonding situation. The endohedral bond distance between the iridium-bonded vertex and that bearing the tetrylene moiety (Si3–Si4 **2a**: 2.549(2) Å, **2b**: 2.565(1) Å) is considerably elongated in comparison to those in the aforementioned chlorosilyltricyclo[2.1.0.0^{2,5}]pentasilane (2.356 Å)[14] and a dianionic Si$_5$ cluster with the same tricyclic scaffold (2.3822 Å).[15]

This is probably a consequence of the back and forth electron transfer between iridium and cluster orbitals, but may also indicate a propellane-like bonding situation as suggested by the hemispheroidality of Si4. On the other hand, Si3 does not fulfill the criterion of hemispheroidality,[8a] but rather adopts a very near planar-tetracoordinate coordination environment instead (**2a**: ϕ(Si3) = −0.0154 Å, ϕ(Si4) = +0.7559 Å; **2b**: ϕ(Si3) = −0.0060 Å, ϕ(Si4) = +0.7276 Å). The bond lengths between the bridgehead silicon atoms Si1 and Si3 in **2a,b** (**2a**: 2.305(2) Å, **2b**: 2.2962(2) Å) are now at the short end of the usual range for silicon single bonds as also observed in the chlorosilyltricyclo[2.1.0.0^{2,5}]pentasilane (2.312 Å).[14] The ^{29}Si CP/MAS spectra of **2a–c** show very similar signals to those in C$_6$D$_6$ solution thus confirming the integrity of the coordination modes upon solvation (the stannylene–Si$_6$ iridium complex **2c** shows a double set of signals due to two crystallographically independent molecules in the asymmetric unit; see ESI†). The longest wavelength absorption bands in the UV/vis spectra at λ_{max} = 576 nm (**2a**), 580 nm (**2b**), 592 nm (**2c**) are strongly redshifted compared to previously reported *ligato*-substituted siliconoids (λ_{max} = 364 to 521 nm).[9,13]

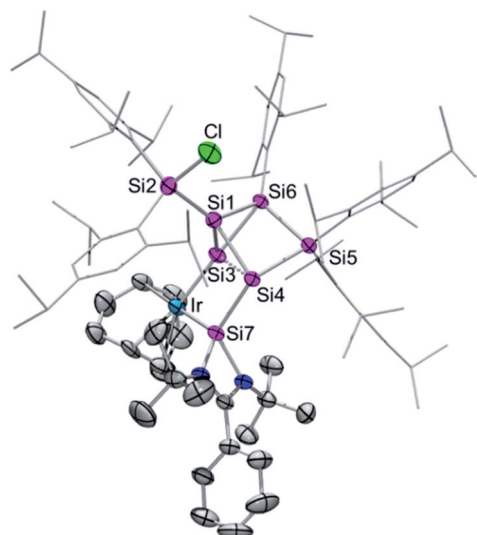**Scheme 1** Synthesis of tetrylene-Si$_6$ iridium complexes **2a–c** from tetrylene-functionalized Si$_6$ siliconoids **1a–c** (**2a**: E = Si, **2b**: E = Ge, and **2c**: E = Sn).

Table 1 Selected ^{29}Si NMR data of **2a–c**, **3**, **4**

| Siliconoid	δ^{29}Si2 [ppm]	δ^{29}Si5 [ppm]	δ^{29}Si6 [ppm]	δ^{29}Si3 [ppm]	δ^{29}Si4 [ppm]	δ^{29}Si7 [ppm]	δ^{29}Si2 solid [ppm]	δ^{29}Si6 solid [ppm]	δ^{29}Si7 solid [ppm]
2a	13.3	55.3	−38.4	−128.2	−126.8	32.9	11.5	−41.6	32.9
2b	12.8	52.6	−41.6	−90.8	−121.7	—	12.3	−41.5	—
2c	12.2	50.6	−42.1	−103.8	−120.2	—	10.2	−42.2	—
3	158.8	−58.3	58.3	165.7	—	108.7	157.3	54.1	107.7
4	162.6	17.6	21.8	—	−9.0	48.2	161.8	14.5	42.7

Fig. 1 Representative molecular structure of silylene-functionalized siliconoid iridium complex **2a** in the solid state. Hydrogen atoms are omitted for clarity. Thermal ellipsoids are set at 50% probability. For structures of **2b,c** see ESI.† Selected bond lengths [Å] and angles [°]: **2a**: Ir−Si7 2.320(1), Ir−Si3 2.334(1), Si1−Si3 2.305(2), Si1−Si4 2.313(2), Si1−Si6 2.364(2), Si1−Si2 2.369 (2), Si3−Si6 2.353(1), Si3−Si4 2.548(2), Si3−Si7 2.764(2), Si4−Si5 2.391(2), Si4−Si7 2.402(2), Si7−N2 1.857(3), Si7−N1 1.884(3), Cl−Si2−Si1 99.03(6), Si1−Si3−Ir 124.02(5), Ir−Si3−Si6 174.93(6), Ir−Si3−Si4 105.99(5), Ir−Si3−Si7 53.33(3), and Si7−Si4−Si3 67.81(4); **2b**: Ir−Si3 2.3517(7), Ir−Ge 2.4113(3), Ge−Si4 2.4444(8), Ge−Si3 2.8481(8), Si1−Si3 2.296(1), Si1−Si4 2.302(1), Si1−Si2 2.356(1), Si1−Si6 2.375(1), Si3−Si6 2.339(1), Si3−Si4 2.565(1), Si4−Si5 2.389(1), Si5−Si6 2.368(1), Ge−N2 1.995(2), Ge−N1 2.005(2); Cl−Si2−Si1 100.91(4), Ir−Si3−Ge 54.243(17), Ir−Si3−Si4 106.90(3), Si6−Si3−Ir 173.61(4), Si1−Si3−Ir 124.75(4), Ir−Ge−Si3 52.322(16), Ir−Ge−Si4 108.95(2), Si3−Ir−Ge 73.436(19), and Ge−Si4−Si3 69.25(3).

Synthesis of rhodium complexes

The reaction of 1 equivalent of bis[(1,5-cyclooctadiene)rhodium(I) chloride] with **1a–c** led to a complicated mixture of products in all cases, presumably due to competing oxidative addition and reductive elimination reactions. In one crystallization attempt of the product mixture from **1b** (E = Ge) a few red-brownish crystals were collected and then investigated by X-ray diffraction showing the same motif as observed in **2a–c** (see ESI†). In the anticipation that it might react in a similar manner despite the differing ligand set, we considered the rhodium(I) dicarbonyl chloride dimer [Rh(CO)₂Cl]₂ as an alternative. The reactions of **1a–c** with 1 equivalent of [Rh(CO)₂Cl]₂, however, led to uniform conversion only in the case of **1a** and inseparable mixtures of products for **1b,c** according to NMR spectra. In addition, ¹H NMR monitoring of the reaction mixture revealed the rearrangement of the initial product overnight in the case of **1a** (Scheme 2).

Treatment of **1a** with 1 equivalent of [Rh(CO)₂Cl]₂ in toluene followed by cooling to −26 °C after three minutes of stirring at ambient temperature yields dark red crystals of the primary product **3** after storage for 2 to 3 h in 56% crystalline yield. Conversely, the secondary product **4** is obtained as red-brownish crystals in 63% yield by crystallization from hexane after stirring the reaction mixture overnight. Both **3** and **4** were
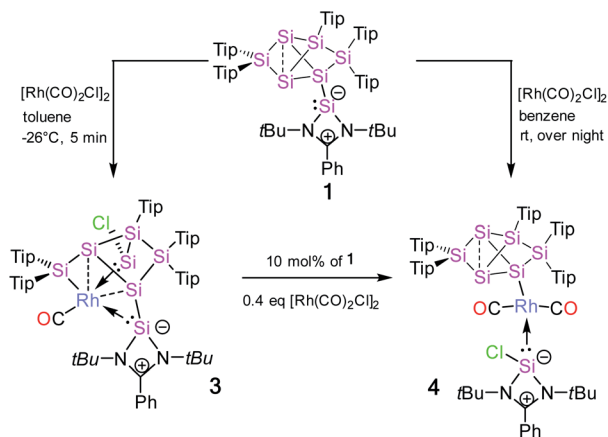
Scheme 2 Synthesis of Si₇ rhodium complexes **3** and **4** from silylene-functionalized Si₆ siliconoid **1**.

fully characterized by multinuclear NMR spectroscopy and X-ray diffraction on single crystals (Fig. 2 and 3).

In contrast to the iridium complexes **2a–c**, the rhodium centre of **3** is fully incorporated into the core structure under expansion to a 7-vertex motif. Only one of the CO ligands is retained in **3** completing the distorted trigonal-pyramidal coordination sphere at rhodium in an apical position (C16–
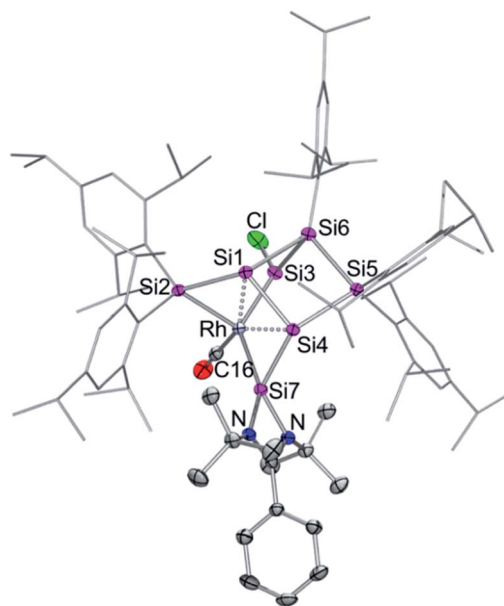
Fig. 2 Molecular structure of silylene-functionalized siliconoid rhodium complex **3** in the solid state. Hydrogen atoms are omitted for clarity. Thermal ellipsoids are set at 50% probability. Selected bond lengths [Å] and angles [°]: Rh−Si3 2.2455(7), Rh−Si7 2.3104(7), Rh−Si5 2.3872(8), Rh−Si2 2.5936(7), Rh−Si1 2.5965(7), Si3−Cl 2.102(1), Si1−Si2 2.279(1), Si1−Si5 2.373(1), Si1−Si4 2.499(1), Si2−Si7 2.254(1), Si2−Si6 2.333(1), Si3−Si4 2.308(1), Si4−Si6 2.401(1), Si7−N1 1.837(2), Si7−N2 1.822(2), Si3−Rh−Si7 132.05(3), Si3−Rh−Si5 97.85(3), Si7−Rh−Si5 116.303, Si3−Rh−Si2 87.62(2), Si7−Rh−Si2 54.36(2), Si5−Rh−Si2 102.19(2), Si3−Rh−Si1 72.23(2), Si7−Rh−Si1 98.48(2), Si5−Rh−Si1 56.69(2), Si4−Si1−Rh 94.98(3), Si7−Si2−Rh 56.40(2), Si1−Si2−Rh 64.02(3), and Si6−Si2−Rh 115.58(3).
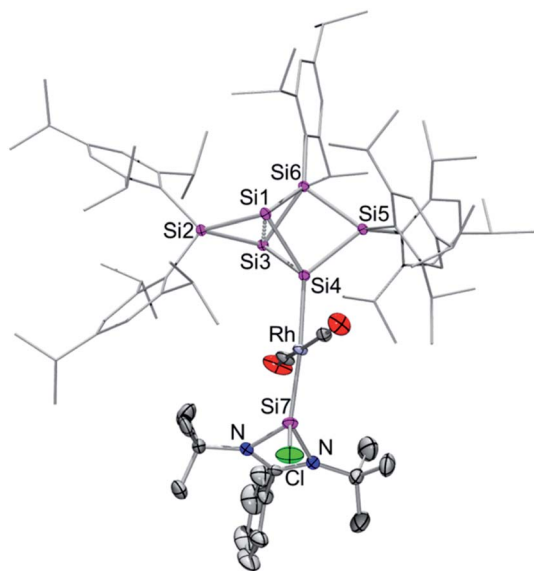
Fig. 3 Molecular structure of silylene-functionalized siliconoid rhodium complex **4** in the solid state. Hydrogen atoms are omitted for clarity. Thermal ellipsoids are set at 50% probability. Selected bond lengths [Å] and angles [°]: Rh–Si7 2.305(1), Rh–Si4 2.398(1), Si3–Si6 2.342(1), Si2–Si3 2.352(1), Si3–Si4 2.386(1), Si1–Si2 2.619(1), Si1–Si4 2.336(1), Si1–Si6 2.351(1), Si1–Si2 2.392(1), Si1–Si3 2.619(1), Si4–Si5 2.384(1), Si5–Si6 2.371(1), Si7–N1 1.826(3), Si7–N2 1.831(3), Si7–Cl 2.077(2), Si7–Rh–Si4 172.63(4), Si3–Si4–Rh 131.22(5), Si5–Si4–Rh 132.67(5), Si1–Si4–Rh 124.01(5), and Si4–Si1–Si2 97.15(5).

Rh–Si2 102.586(4)°, C16–Rh–Si3 104.881(5)° 45.489(4)°, centre(Si1–Si4)–Rh–Si2 79.149(4)°, centre(Si1–Si4)–Rh–Si3 78.869(4)°, centre(Si1–Si4)–Rh–Si7 75.997(4)°, C16–Rh–centre(Si1–Si4) 175.493(6)°, and Si7–Rh–Si3 132.095(5)°). The geometric parameter $\tau = (\beta - \alpha)/60$ is commonly used for pentacoordinate complexes as an index of the degree of the trigonality in trigonal-bipyramidal and square-planar pyramidal structural motifs.[17] With the two largest angles α and β of **3** (β: C16–Rh–centre(Si1–Si4) 175.493(6)°; α: Si7–Rh–Si3 132.095(5)°) the angular parameter is $\tau = 0.72$ in line with a distorted trigonal-bipyramidal coordination sphere of Rh. The chlorine atom is shifted to one of the former *nudo*-vertices so that the extrusion of the *privo*-SiTip$_2$ moiety as in **2a–c** is avoided in this case. Intriguingly, the chloro-substituted silicon vertex (Si3) is conferred a significant silylene character: the corresponding bond distance to rhodium (Si3–Rh 2.2455(7) Å) is considerably shorter than that of the amidinato silylene moiety, which binds to rhodium at a distance (Si7–Rh 2.3104(7) Å) similar to those reported for other complexes with this motif.[5,16e] The former *privo*-vertex binds to the Rh centre at a distance (Si2–Rh 2.3872(8) Å) in line with the covalent radii of silicon and rhodium. Si2, Si3 and Si7 bind in equatorial positions and thus form the base of the trigonal-bipyramidal coordination environment at Rh.

The Si1–Si4 bond is unusually short (2.279(1) Å) and occupies the remaining apical positions at Rh at relatively long distances (Si4–Rh 2.5936(7) Å and Si1–Rh 2.5965(7) Å). Both Si1 and Si4 exhibit a hemispheroidal coordination environment

with hemispheroidalities of $\phi(Si1) = +0.8003$ Å and $\phi(Si4) = +0.4764$ Å.[8a] The degree of the metallacyclopropane character of this coordinating interaction according to the Dewar–Chatt–Duncanson model[18] is difficult to estimate due to the complexity of the bonding situation as Si1–Si4, albeit shorter than a usual single bond, is heavily involved in cluster bonding.

The ^{29}Si NMR spectrum in C$_6$D$_6$ is consistent with the bonding situation as discussed on the basis of the solid state structure. Four of the seven resonances are split into doublets by the coupling to the ^{103}Rh nucleus suggesting the coordination of rhodium being uncompromised by solvation. The signals are, however, not as broadly dispersed as typically observed for Si$_6$ siliconoids.[9,13] The former *privo*-vertex Si2 gives rise to a low-field ^{29}Si NMR signal, albeit it splits into a doublet at 158.8 ppm with a coupling constant of $J^{29}(Si,^{103}Rh) = 41.0$ Hz. The silylene character of the former *nudo*-vertex Si3, now bearing the chloro substituent, results in the significant deshielding of the corresponding ^{29}Si NMR signal at 165.7 ppm. The interaction with the rhodium centre is reflected in the coupling constant of $J^{29}Si,^{103}Rh = 53.4$ Hz. The ^{103}Rh coupling of the two hemispheroidally coordinated vertices Si1 and Si4 is too small to resolve resulting in singlets at −140.2 and −122.1 ppm. Although a discussion of the magnitude of experimental coupling constants is next to impossible in polycyclic systems such as **3** the absence of detectable coupling is in line with a predominant π-character of the coordination to rhodium.[3a] The assignment is backed by the absence of cross-peaks to Tip groups in the 2D ^{29}Si/^{1}H correlation. The doublet at 108.7 ppm ($J^{29}Si,^{103}Rh = 59.6$ Hz) is assigned to the N-heterocyclic silylene moiety (Si7) based on the observation of a cross-peak to the *t*-butyl groups. In notable contrast, the signal of the not directly Rh-bonded Si6 at 58.3 ppm (assigned on the basis of a cross-peak to one Tip substituent) is split into a doublet with $J^{29}Si,^{103}Rh = 14.3$ Hz.

Surprisingly, after the rearrangement of Rh(ı) complex **3** to **4**, the diagnostic wide dispersion of ^{29}Si NMR shifts is again observed, which suggested the re-establishment of an uncompromised benzpolarene[9,13] scaffold. Besides the characteristic highfield resonances for the *nudo*-vertices Si1 and Si3 at −256.1 and −258.3 ppm, the ^{29}Si NMR signal of the tetracoordinate *privo*-vertex Si2 appears at the typical low field at 162.6 ppm. The doublet in the ^{29}Si NMR at 48.2 ppm with $J^{29}Si,^{103}Rh = 84.5$ Hz is attributed to the N-heterocyclic silylene moiety on the basis of a cross-peak to the *t*-butyl groups in the 2D ^{29}Si/^{1}H correlation and the large coupling indicative of pronounced s-orbital contributions. In contrast, the doublet at −9.0 ppm with $J^{29}Si,^{103}Rh = 31.5$ Hz suggests a covalent bond to the ^{103}Rh nucleus. Due to the absence of a cross-peak to a Tip group in the 2D ^{29}Si/^{1}H correlation NMR spectrum, it can be attributed to the *ligato*-vertex Si4. The remaining ^{29}Si NMR chemical shifts are located in the usual range of saturated silicon atoms; only one of the signals showing a small coupling to the Rh centre (21.8 ppm; $J^{29}Si,^{103}Rh = 8.5$ Hz). The anticipated structure of **4** as an uncompromised benzpolarene scaffold covalently attached to rhodium was confirmed by X-ray diffraction in the solid state (Fig. 3).

The rhodium centre of **4** exhibits a typical square-planar coordination environment, with the hexasilabenzpolarene moiety indeed connected through the *ligato*-position Si4. Astonishingly, not only has the Si_6 moiety been reinstated during the isomerization from **3**, but the amidinato silylene – now disconnected from the siliconoid and coordinated to the rhodium centre in a *trans*-fashion – has reacquired its chloro-substituent as well. The coordination at the rhodium centre is completed by two CO ligands, which requires the "come-back" of the initially dissociated CO molecule. The Si7–Rh bond length of 2.305(1) Å is in line with the reported donor–acceptor bond length of Si–Rh complexes.[5,16e] Interestingly, it is significantly shorter than the covalent Si4–Rh bond length of 2.398(1) Å in the same molecule. The distance between the bridgehead silicon atoms (Si1–Si3 2.6188(4) Å) is similar to that in previously reported *ligato*-substituted Si6 siliconoids.[9,13] The longest wavelength absorption bands are observed at $\lambda_{max} = 461$ nm (**3**) and 466 nm (**4**) and thus are slightly blue-shifted compared to the *ligato*-metalated siliconoids Zr and Hf (Zr: 521 nm, Hf: 497 nm).[13] The Rh complexes **3** and **4** exhibit IR characteristics of rhodium carbonyl complexes[19] with CO stretching modes at $\nu = 1978$ cm^{-1} (**3**) and 1951, 1949 cm^{-1} (**4**).

Mechanistic considerations

Due to the flexibility of the coordination environments, reactions involving transition metals generally proceed through multiple steps and, consequently, the mechanisms are often complicated, especially when backbone structures are reconstructed such as in the present case through a sequence of cleavage and formation of Si–Si bonds. Although, a computational treatment of such mechanisms is well out of reach to us due to the anticipated complexity of the potential energy surfaces and the large size of the involved molecules, we propose a plausible mechanism for the Ir and Rh structures based on the structurally characterized products (Chart 1).
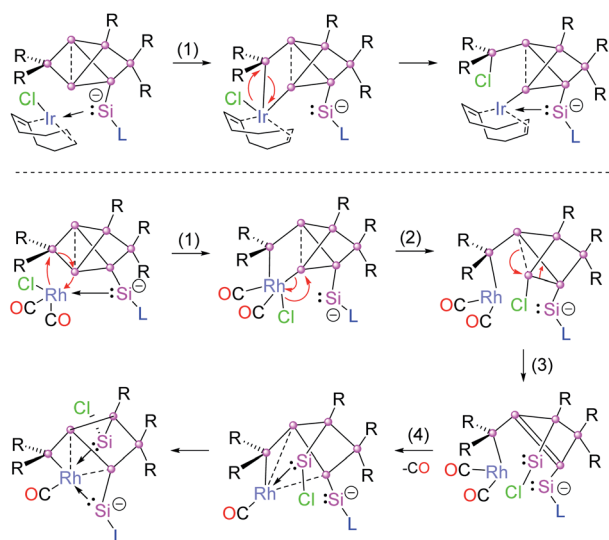

Chart 1 Proposed mechanism of the formation of **2a** (top) and **3** (bottom).

All reactions are likely initiated by the straightforward coordination of the pendant silylene ligand to the metal. For the subsequent rearrangements, we suggest the oxidative addition to the Si2–Si3 single bond as the common first step (step 1 in Chart 1). From the second step onwards, however, the isomerizations proceed through distinct pathways for the rhodium and iridium species. In the case of **2a**, the oxidative addition is directly followed by reductive elimination of the chloro group and the $SiTip_2$ moiety from the Ir centre resulting in the formation of the exohedral chlorosilyl group in the final product **2a** (and by extension **2b,c**). In contrast, in the case of the primary rhodium product **3** the chlorine migrates to Si3 (step 2). In step 3, the formation of the chlorosilylene Si3 is suggested, while a formal double bond between Si1–Si4 is formed as a consequence. In the last step, the final product **3** is formed by elimination of a CO unit enforced by the coordination of the Si1–Si4 bond and the silylenes (Si3 and Si7) to the Rh centre. The question of the re-establishment of the intact hexasilabenzpolarene scaffold from intermediate **3** to yield the final product **4** is even more daunting as it requires the return of the previously eliminated CO ligand into the coordination sphere of rhodium. Notably, a solution of crystallized **3** turned out to be inert towards exposure to CO atmosphere as well as the addition of excess $[(CO)_2RhCl]_2$. We therefore assumed that the formation of **4** can only be attained by a reactive species formed *in situ* during the reaction of **1a** with $[(CO)_2RhCl]_2$. Indeed, treatment of a solution of isolated crystals of **3** with 10 mol% of silylene-substituted siliconoid **1a** and 0.4 equivalents of additional $[(CO)_2RhCl]_2$ results in the uniform conversion of isolated **3** to **4** in the course of 24 h. We speculate that either an extremely short-lived intermediate of monomeric $[(CO)_3RhCl]$[20] or a heterodimer not unlike the one reported by Braunschweig *et al.*[21] might be responsible for the CO delivery.

Alkene isomerization catalysis

Despite the plethora of synthetic methods available for the introduction of C–C double bonds, the regioisomerization of an existing C–C double bond is a viable alternative.[22] The so-called alkene isomerization, however, results in mixtures of (*E*) and (*Z*)-alkenes in many cases[23] or further migration along a saturated carbon chain. The selective transformation of terminal alkenes to 2-alkenes has thus attracted considerable interest.[24] We anticipated that electron-rich siliconoid ligands might fulfil two functions in a homogenous catalyst for alkene isomerization: (a) acting as an electron reservoir and thus facilitating oxidative addition reactions and (b) providing sufficient steric bulk to improve the selectivity regarding the number of positions the C–C double bond migrates. We therefore probed the isomerization of terminal alkenes to 2-alkenes in the presence of catalytic quantities of complexes **2a–c**, **3** and **4**.

As rapidly indicated by first preliminary tests, no solvent is required for the catalytic activity of **2a–c**, **3** and **4** and therefore all runs were carried out with the neat substrate, an attractive feature from both ecologic and economic perspectives. Allyl-trimethylsilane and 1-hexene were used as neat substrates on an NMR scale using a C_6D_6 capillary as the locking signal; yields

Table 2 Reaction conditions, conversion determined by ^{1}H NMR spectroscopy

Catalyst	Substrate	Cat. loading [mol%]	Time [h]	Temperature [°C]	Σ conversion [%]	E-isomer [%]	Z-isomer [%]	TON	TOF [h^{-1}]
2a	1-Hexene	0.05	16	25	95	—	—	1902.7	118.9
2b	1-Hexene	0.1	72	25	97	—	—	968.8	13.5
2c	1-Hexene	0.1	100	25	75	—	—	748.4	7.5
2a	Allyl-SiMe$_3$	0.8	26	60	94	77	17	117.4	4.5
2b	Allyl-SiMe$_3$	0.8	30	60	89	73	16	111.6	3.7
2c	Allyl-SiMe$_3$	0.8	30	60	78	63	15	97.4	3.2
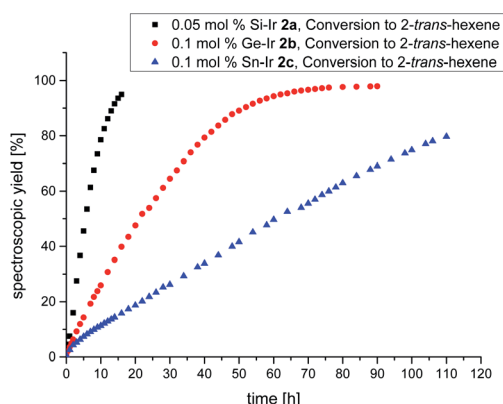
Fig. 4 Plot of the spectroscopically determined conversion to 2-*trans*-hexene. Black = Si–Ir **2a** (0.05 mol%), red = Ge–Ir **2b** (0.1 mol%), and blue = Sn–Ir **2c** (0.1 mol%).

were calculated from ^{1}H NMR integrations (Table 2). Fig. 4 shows the spectroscopic conversion to 2-*trans*-hexene using 0.05 mol% (**2a**), 0.1 mol% (**2b**, **2c**) of the catalysts at room temperature as a function of time. The side chain migration to 3-*trans*-hexene is disregarded in the plots due to the overlap of the chemical shifts, and estimated to be <10% from the spectroscopic data. Blind tests without catalyst or in the presence of [(cod)IrCl]$_2$ or [(CO)$_2$-RhCl]$_2$ led to no detectable conversion under identical conditions. The reaction can therefore easily be quenched after the formation of 2-*trans*-hexene is complete by simple addition of
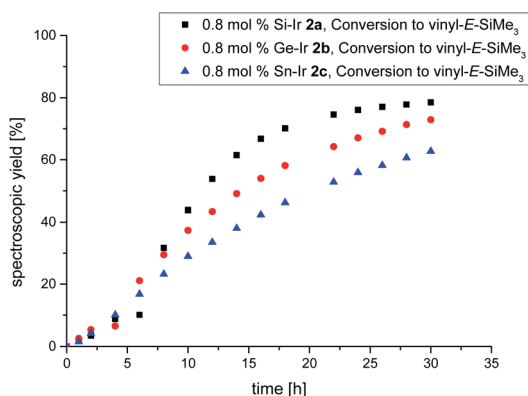
Fig. 5 Plot of the spectroscopically determined conversion to E-vinyltrimethylsilane 60 °C using the 0.8 mol% catalyst. Black = Si–Ir **2a**, red = Ge–Ir **2b**, blue = Sn–Ir **2c**.

water leading to the hydrolysis of the catalyst. The catalytic performance is best in the case of **2a** (E = Si, TOF = 119 h^{-1}) with catalyst loadings as low as 0.05 mol% and strongly decreases from **2b** (E = Ge, TOF = 13.5 h^{-1}) to **2c** (E = Sn, TOF = 7.5 h^{-1}) both requiring double catalyst loads. Preliminary results show a much lower catalytic activity of the rhodium complexes **3** and **4** which was therefore not investigated in detail (see ESI†). The isomerization of allyltrimethylsilane to 2-E/Z-vinyltrimethylsilane proceeds significantly slower even with the more active **2a–c** and requires higher temperatures as well as one order of magnitude larger amounts of catalyst (0.8 mol%, 60 °C, Fig. 5, ESI†).

It should be noted, however, that the reaction at room temperature is probably slowed down even further due to the moderate solubility of the crystalline samples of the catalysts **2a–c** in neat allyltrimethylsilane. This phenomenon is manifest in an extended induction period of approximately 5 h (Fig. 5) after which the spectroscopic yield increases much faster due to rapid dissolution in the mixture of allyltrimethylsilane and the isomerization products.

The driving force of the alkene isomerization is the higher thermodynamic stability of internal alkenes.[25] As suggested by the negative blind tests with the siliconoid-free precursors, the intramolecular hydrogen migration is supported through the extremely electron-rich hexasilabenzpolarene scaffold.

Conclusion

In conclusion, with the Group 9 metal complexes **2a–c** and **3** we reported the first siliconoids with endohedral incorporation of transition metals. As demonstrated by the isomerization of **3** to the **4** with complete reconstitution of the uncompromised benzpolarene scaffold, a temporary change in the coordination mode of these ligands is possible in principle. All isolated complexes show catalytic activity in the isomerization of alkenes with the best (**2a**) reaching competitive selectivity at satisfactory conversion rates in the case of 1-hexene.

Conflicts of interest

There are no conflicts to declare.

Acknowledgements

Notes and references

1 Recent reviews: (*a*) E. Rivard, *Chem. Soc. Rev.*, 2016, **45**, 989–1003; (*b*) B. Blom and M. Driess, Functional Molecular Silicon Compounds II, in *Structure and Bonding*, ed. D. Scheschkewitz, 2013, vol. 156, pp. 85–123; (*c*) S. Mandal and H. W. Roesky, *Acc. Chem. Res.*, 2012, **45**, 298–307; (*d*) M. Asay, C. Jones and M. Driess, *Chem. Rev.*, 2011, **111**, 354–396; (*e*) Y. Mizuhata, T. Sasamori and N. Tokitoh, *Chem. Rev.*, 2009, **109**, 3479–3511.

2 Recent reviews: (*a*) A. Rammo and D. Scheschkewitz, *Chem.–Eur. J.*, 2018, **24**, 6866–6885; (*b*) T. Matsuo and N. Hayakawa, *Sci. Technol. Adv. Mater.*, 2018, **19**, 108–129; (*c*) C. Präsang and D. Scheschkewitz, *Chem. Soc. Rev.*, 2016, **45**, 900–921; (*d*) T. Iwamoto and S. Ishida, Functional Molecular Silicon Compounds II, in *Structure and Bonding*, ed. D. Scheschkewitz, 2013, vol. 156, pp. 125–202.

3 Recent reviews: (*a*) S. Ishida and T. Iwamoto, *Coord. Chem. Rev.*, 2016, **314**, 34–63; (*b*) S. Raoufmoghaddam, Y.-P. Zheng and M. Driess, *J. Organomet. Chem.*, 2017, **829**, 2–10; (*c*) B. Blom, M. Stoelzel and M. Driess, *Chem.–Eur. J.*, 2013, **19**, 40–62.

4 (*a*) A. Brück, D. Gallego, W. Wang, E. Irran, M. Driess and J. F. Hartwig, *Angew. Chem., Int. Ed.*, 2012, **51**, 11478–11482; (*b*) B. Blom, D. Gallego and M. Driess, *Inorg. Chem. Front.*, 2014, **1**, 134–148.

5 M. Stoelzel, C. Präsang, B. Blom and M. Driess, *Aust. J. Chem.*, 2013, **66**, 1163–1170.

6 (*a*) D. Gallego, A. Brück, E. Irran, F. Meier, M. Kaupp, M. Driess and J. F. Hartwig, *J. Am. Chem. Soc.*, 2013, **135**, 15617–15626; (*b*) M. Zhang, X. Liu, C. Shi, C. Ren, Y. Ding and H. W. Roesky, *Z. Anorg. Allg. Chem.*, 2008, **634**, 1755–1758.

7 B. Blom, S. Enthaler, S. Inoue, E. Irran and M. Driess, *J. Am. Chem. Soc.*, 2013, **135**, 6703–6713.

8 Reviews: (*a*) Y. Heider and D. Scheschkewitz, *Dalton Trans.*, 2018, **47**, 7104–7112; (*b*) S. Ishida and T. Iwamoto, *Chem. Lett.*, 2014, **43**, 164–170.

9 (*a*) P. Willmes, K. Leszczyńska, Y. Heider, K. Abersfelder, M. Zimmer, V. Huch and D. Scheschkewitz, *Angew. Chem., Int. Ed.*, 2016, **55**, 2907–2910; (*b*) Y. Heider, N. E. Poitiers, P. Willmes, K. I. Leszczyńska, V. Huch and D. Scheschkewitz, *Chem. Sci.*, 2019, **10**, 4523–4530.

10 (*a*) S. Scharfe, F. Kraus, S. Stegmaier, A. Schier and T. F. Fässler, *Angew. Chem., Int. Ed.*, 2011, **50**, 3630–3670; (*b*) J. M. Goicoechea and S. C. Sevov, *Organometallics*, 2006, **25**, 5678–5692.

11 Recent review: R. J. Wilson, B. Weinert and S. Dehnen, *Dalton Trans.*, 2018, **47**, 14861–14869.

12 Recent review: (*a*) S. D. Hoffmann and T. F. Fässler, *Angew. Chem., Int. Ed.*, 2004, **43**, 6242–6247; (*b*) K. Mayer, J. Weßing, T. F. Fässler and R. A. Fischer, *Angew. Chem., Int. Ed.*, 2018, **57**, 14372–14393.

13 N. E. Poitiers, L. Giarrana, K. I. Leszczyńska, V. Huch, M. Zimmer and D. Scheschkewitz, *Angew. Chem., Int. Ed.*, 2020, **59**, 8532–8536.

14 K. Abersfelder, A. Russell, H. S. Rzepa, A. J. P. White, R. Haycock and D. Scheschkewitz, *J. Am. Chem. Soc.*, 2012, **134**, 16008–16016.

15 Y. Heider, P. Willmes, V. Huch, M. Zimmer and D. Scheschkewitz, *J. Am. Chem. Soc.*, 2019, **141**(49), 19498–19504.

16 (*a*) M. Kilian, H. Wadepohl and L. H. Gade, *Organometallics*, 2008, **27**(4), 524–533; (*b*) A.-K. Jungton, A. Meltzer, C. Präsang, A. Penner, T. Braun and M. Driess, *Dalton Trans.*, 2010, **39**, 5436–5438; (*c*) D. O. Downing, P. Zavalij and B. W. Eichhorn, *Eur. J. Inorg. Chem.*, 2010, 890–894; (*d*) A. Wagenpfeil, C. Nickl, H. Schubert, K. Eichele, M. A. Fox and L. Wesemann, *Eur. J. Inorg. Chem.*, 2011, 3349–3356; (*e*) S. Kaufmann, S. Schäfer, M. T. Gamer and P. W. Roesky, *Dalton Trans.*, 2017, **46**, 8861–8867; (*f*) B. Su, K. Ota, Y. Li and R. Kinjo, *Dalton Trans.*, 2019, **48**, 3555–3559; (*g*) K. M. Krebs, S. Freitag, J.-J. Maudrich, P. Sirsch and L. Wesemann, *Dalton Trans.*, 2018, **47**, 83–95.

17 A. W. Addison and T. N. Rao, *J. Chem. Soc., Dalton Trans.*, 1984, 1349–1356.

18 (*a*) M. J. S. Dewar, *Bull. Soc. Chim. Fr.*, 1951, **18**, C71; (*b*) J. Chatt and L. A. Duncanson, *J. Chem. Soc.*, 1953, 2939–2947.

19 D. K. Dutta and M. M. Singh, *Transition Met. Chem.*, 1979, **4**, 230–234.

20 M. P. Keyes and K. L. Watters, *J. Catal.*, 1986, **100**, 477–481.

21 K. Radacki, M. Forster and H. Braunschweig, *Angew. Chem., Int. Ed.*, 2006, **45**, 2132–2134.

22 G.-J. Boons, A. Burton and S. Isles, *Chem. Commun.*, 1996, 141–142.

23 G. Chahboun, C. E. Petrisor, E. Gómez-Bengoa, E. Royo and T. Cuenca, *Eur. J. Inorg. Chem.*, 2009, 1514–1520.

24 (*a*) R. H. Grubbs, *Tetrahedron*, 2004, **60**, 7117–7140; (*b*) C. R. Larsen and D. B. Grotjahn, *J. Am. Chem. Soc.*, 2012, **134**, 10357–10360; (*c*) C. Chen, T. R. Dugan, W. W. Brennessel, D. J. Weix and P. L. Holland, *J. Am. Chem. Soc.*, 2014, **136**, 945–955; (*d*) J. Becica, O. D. Glaze, D. I. Wozniak and G. E. Dobereiner, *Organometallics*, 2018, **37**, 482–490.

25 D. B. Dahl, C. Davies, R. Hyden, M. L. Kirova and W. G. Lloyd, *J. Mol. Catal. A: Chem.*, 1997, **123**, 91–101.